Topological dislocations for plasmonic mode localization

Eliav Epstein
Ariel University
Leeju Singh
Ariel University
Maayan Fox
Ariel University
Shmuel Sternklar
Ariel University
Yuri Gorodetski (ygorodetski@gmail.com)
Ariel University

Article

Keywords: Line Defects, Point Singularities, Near Field Distributions

Posted Date: October 7th, 2020

DOI: https://doi.org/10.21203/rs.3.rs-84321/v1

Topological dislocations for plasmonic mode localization.

Eliav David Epstein[1,+], Leeju Singh[1,+], Maayan Fox[1,2,+], Shmuel Sternklar[2], and Gorodetski Yuri[1,2,*]

[1]Department of Electrical and Electronic Engineering, Ariel University, Ariel, 407000

[2]Department of Mechatronics and Mechanical Engineering, Ariel University, Ariel, 407000

[*]yurig@ariel.ac.il

[+]these authors contributed equally to this work

ABSTRACT

We study the localization of plasmonic modes on topological dislocations obtained by an abrupt change in the geometry of unit-cells in a plasmonic metasurface. We experimentally demonstrate mode localization in line defects and point singularities in the topology. These results are confirmed by numerical simulations of the near field distributions along the topology boundaries. We present structures with line dislocations supporting dark and bright modes. Moreover, we show that in structures with point dislocations the localization strength can be further manipulated by modifying the topological order of the structure.

Introduction

The field of topological photonics[1–4] has gained much interest lately in nanophotonics and optical communication communities[5,6]. Topology[7,8] has, in fact, been recognized as a novel degree of freedom in light-matter interactions as it provides an almost lossless medium for optical signals. Efficient light confinement, guiding and localization have been achieved by using photonic crystal[9] (PhC) optical systems with topological states[10]. These optical modes have emerged within the photonic band-gap[11] induced by the PhC periodicity at an interface between two or more regions with different topological phases[1,12]. The optical edge states were shown to be topology protected and propagated with negligible scattering losses, in analogy with currents in so-called topological insulators that have been recently discovered[13,14]. Modern nano-fabrication techniques facilitate the realization of nanoscale periodic optical media with any desired geometry, which provides a practical advantage for the topology based nanophotonics with respect to a classical index-modulated systems[11,15]. A special interest was focused on systems supporting surface plasmon (SP)[16,17] modes - excitations of the bound electric charges in the vicinity of a metal-insulator interface. It has already been shown that these excitations are intrinsically topological in nature, and represent an edge state[18–20] of two adjacent media with an abrupt sign change of the dielectric constant. Nevertheless, some further studies have discussed the possibility of further localizing the SP modes within a metasurface - the 2D equivalent of a metamaterial comprising a periodic structure with effective optical properties. Most commonly, such a system is realized via nanometric apertures or particles periodically arranged on a metal surface. Similarly to the aforementioned PhC, a specially designed doubly periodic metasurface can behave as a plasmonic crystal (PlC) with an accurately designed band-gap,

where intentionally produced defects can localize and guide the SPs[21,22]. Various configurations of PlC have been proposed for a variety of nanooptics applications[23,24]. It has been shown that such a mechanism provides a promising platform for future nanophotonic circuitry as well as various active plasmonic devices such as lasers and sensors[25–27]. It has also been demonstrated that exciting SPs by means of an anisotropic scatterer can lead to the geometric Berry phase that can further modify the propagation conditions of the surface waves[28–30]. The Berry phase has a topological origin as it stems from the light's polarization manipulation defined by a path on a configurational space represented by the Poincare sphere[31,32]. In this context, one may inquire whether the abrupt change of the Berry phase induced in the plasmonic metasurface may lead to the topological edge states. In this paper we demonstrate the appearance of such plasmonic edge states at the boundary between two zones of a PlC with different topological phases. We design a Bragg type plasmonic medium where no propagating SP modes are allowed. We use anisotropic rectangular apertures as the metasurface unit cell and excite it by circularly polarized light. This configuration enables us to manipulate the topological phase of the excited modes that can be simply controlled by the aperture angular orientation. We experimentally investigate a number of plasmonic metasurfaces comprised of two domains with an abrupt change in topology - a topological dislocation. Here we discuss line and point dislocations with trivial and non-trivial topological phases. Our leakage radiation (LR) microscopy system allows us to track the excited SP modes directly. Our experimental results and numerical simulations indicate the appearance of plasmonic dark and bright modes at the domain boundaries while their localization properties result solely from the topology.

Experimental evidence of topology protected edge state

Our proposed metasurface was a square array of rectangular apertures fabricated using focused ion beam (FIB) in a $100nm$-thick gold film evaporated on a glass substrate. The structure was comprised of two domains with a relative aperture orientation difference of $\pi/2$ as shown in the conceptual scheme in Fig. 1a. The grating period was designed according to the Bragg condition $d = \frac{\lambda_0}{2}\sqrt{\frac{1+\varepsilon_m}{\varepsilon_m}}$ with respect to the incident wavelength λ_0 (here ε_m is the dielectric constants of gold).

The sample was illuminated by a laser at $\lambda_0 = 780nm$ whose beam polarization had been controlled using a set of polarizer (P) and quarter-wave plate (QWP) and focused by an objective (O1) onto the structure (Figs. 1b). The imaging objective (O2) that was brought into contact with the back side of the sample by means of an index-matching oil produced leakage radiation from the near-field plasmonic signal[33]. This light then passed through a series of imaging lenses L1-L3 and a final image of the SP mode was captured by the camera.

We started with a sample where the apertures had a constant orientation of $+45^\circ$ in its upper half and -45° in the lower half. In Figs. 2a, b a scanning electron microscope (SEM) image of the fabricated sample is presented. The boundary where the aperture orientation changes is marked by the dashed line in the inset. Figures 2c, d show the transmission through the sample captured in our LR system when the illuminating beam was linearly polarized at $\pm 45^\circ$ respectively. By comparing the transmission intensity distribution one can conclude that, as expected, the aperture anisotropy leads to the strong polarization dependence. We then switched to the circularly polarized (CP) illumination. We used an additional set of polarizing elements to filter out the desired polarization state. Moreover, a spatial filter (SF) was placed in the intermediate Fourier plane of the system in order to block the directly propagating light.

In Figs. 2e, f we show the SP distribution measured in our LR system for incident right and left CP state respectively. Here we notice some intensity localization along the boundary between the domains. We can also recognize fringes appearing

parallel to the boundary (indicated on the figure by the white arrow).

We simulated the interaction of the optical field with the structure using Comsol Multiphysics ®software. In Fig. 3a the field amplitude in the vicinity of the metal surface is shown. First, it is clearly visible that each of the apertures indeed behaves as a localized SP source. Nevertheless, due to the Bragg periodicity[10,34] the field decays rapidly everywhere except at the domain boundary. The abrupt change in the aperture orientation behaves as a defect in the Bragg grating, inducing SP scattering similar to the one expected from a single groove. The fringes parallel to the boundary decay as they recede from it, indicating that the momentum of the plasmonic wave is preferably normal to the dislocation. From these results one can deduce that the topological dislocation behaves as a defect in the Bragg grating, generating significant light scattering in the normal direction, with partial coupling to the SP waves that propagate away with a strong amplitude decay. This effect is achieved in our system thanks to the specific phase matching conditions arising along the boundary.

To elucidate the physical mechanism of the system we consider the geometric Berry phase[32]. In general the geometric phase, also known as the Pancharatnam-Berry phase, arises as a result of the polarization state manipulation leading to the closed path on the Poincaré sphere[31,35,36]. Numerous applications and physical system based on this effect have been demonstrated in the last few decades in optics and plasmonics[37,38]. It has been shown that the geometric phase emerges from the holonomy of the system's configurational space, therefore its origin is purely topological. Specifically, in our plasmonic system we consider the rectangular apertures as sources of the localized SPs excited by the incident light scattering. The incident CP light scattered at the rectangular aperture is predominantly linearly polarized according to the local orientation of the scatterer, θ. In the CP basis the light emanating from each aperture is represented as a sum of the original circular component and one with a flipped handedness with an additional geometric phase of $\phi_g = 2\theta$[39,40]. These local scatterers excite SP waves propagating on the surface between the apertures that can serve as the coupling channel. In our metasurface the Bragg periodicity leads to the destructive interference of the propagating SPs as long as the orientation of the apertures is constant. However, once the orientation of the apertures is changed the corresponding geometric phase is added. As schematically shown in Fig. 4, the local polarization state manipulation in each domain is represented by a different path on the Poincaré sphere, resulting in the relative geometric phase equal to half the area enclosed by the paths. We designed the grating such that the aperture orientation change between the two adjacent domains is $\pi/2$ which induces an additional π-phase. Accordingly, the locally excited SPs at the boundary of the two topological domains can now constructively interfere. This provides the condition for excitation of the SP mode that can propagate along the boundary as long as the topology of the domains is maintained.

The light localization found in the first experiment is mostly contributed from the light scattered from the topological boundary. However, we note that the normally incident planewave does not posses the necessary momentum to launch the plasmonic waves along the boundary, and the edge state appears as a "dark" mode. This can also be deduced from the simulated field distribution in Fig. 3a having a minimum intensity at the boundary. The plasmonic waves scattered from the line dislocation seem to propagate away towards the edges of the sample. To obtain the conditions for exciting the SP bright mode we designed another structure comprising of two domains as before but having a zig-zag type boundary (see Fig. 3b and Fig. 5a). In this fashion, every aperture along the boundary is rotated by $\pi/2$ radians with respect to the next one and the total phase between them is then matched. When we illuminate this structure by the incident CP light the boundary itself leads to launching of the SP modes in both directions along the topological dislocation (see Fig. 5b). We have tested a structure with two equal topological domains occupying the upper and the lower halves and also a structure in which one of the domains occupies just a

quarter of the total grating (Fig. 5). In both cases the experimental pictures show a very pronounced mode localization along the line dividing the domains, regardless of its geometry, as should be expected from a topologically protected state. Unlike the previous case, the fringes appearing at the boundary indicate that the momentum of the excited mode is now aligned with the dislocation. We used a Matlab solver particularly designed to calculate the SP fields based upon Huygens principle[41] where each aperture was represented as a point source of SP waves. When we deliberately introduce a π phase jump that is expected as a result of the topology dislocation, we obtain distributions that are significantly similar to the experimental results (see Fig. 5c, f). The edge plasmonic mode seems to be strongly localized along the boundary in both simulated cases.

Plasmonic states with non trivial topology

We decided to extend our study to structures with radial geometry. First we designed a metasurface where the $+45^\circ$ domain has a circular shape in the center of the structure while outside of this area the aperture orientation was -45°. Clearly, the distance between the unit-cells along the boundary is no longer fixed at half the SP wavelength which leads to weaker localization. Nevertheless, one can still recognize a rather pronounced edge mode appearing along the circle circumference (Fig. 6b). At the next stage we introduced a slow θ variation along the azimuthal angle - φ. In particular we let the aperture orientation change as $\theta(\varphi) = m\varphi/2$, where m is the topological order keeping the same abrupt $\pi/2$ change along the circular boundary (Fig. 6d). Here we show the results of the structure with $m = 2$ which expected to induce the overall vortex-type geometric phase of $\phi = 4\varphi$[42]. Interestingly, in the center of the structure, where the phase has a singularity we notice a very strong flower-like light localization (Fig. 6e). Similarly to the topological line dislocation – the boundary along which the π rotation of the aperture occurs – here we observe a point dislocation due to the phase structure. However, as these singularities appear in the plasmonic Bragg grating, they appear as constructive interference and localize light. The difference between these two cases is that the line dislocation suggests a local topological defect while the appearance of the point dislocation is induced by a global azimuthal phase gradient.

The last experiment was performed with a metasurface having the same azimuthal phase ramp as before, but this time the topology change occurred in a square domain at a corner of the sample (see Fig. 6g). When this structure was illuminated by circularly polarized light the line singularity could be easily detected by the excited plasmonic state along the domain edge (Fig. 6h). In addition, we could also measure the point dislocation at the center of the structure exactly at the Berry phase singular point. The excited mode in this case seems to be much more pronounced, strengthening the hypothesis that the presence of this point may act as a SP launcher. The three latter cases were also simulated using our Matlab solver and produced quite similar results (Fig. 6c, f, i). Moreover, combining topological singularities of different types might pave the way for more sophisticated nanophotonic circuitry and other practical devices for optical communication.

It should be noted, that in the current configuration the system is degenerate with respect to the incident circular state. In other words, both circular polarizations lead to the same mode excitation, propagating in both directions equally, as can be seen in the first experiment. The reason for this is the trivial (constant) topological phase induced in both domains. We believe that smart engineering of the phases can lift the spin degeneracy, however this requires more complex metasurface design.

Summary

We have demonstrated the excitation of the edge plasmonic states along the domain boundary on a metasurface. The origin of these states is purely topological, as it stems from the abrupt change of the unit-cell geometry leading to the quantal geometric Berry phase generation. We have shown that some of our structures can support dark or bright SP modes that are topology protected within the metasurface. By using non-trivial (space variant) topological phase we were able to generate a point dislocation which was then shown to localize the SP waves.

References

1. Lu, L., Joannopoulos, J. D. & Soljačić, M. Topological photonics. *Nat. Photonics* **8**, 821–829 (2014).
2. Khanikaev, A. B. & Shvets, G. Two-dimensional topological photonics. *Nat. Photonics* **11**, 763–773 (2017).
3. Ozawa, T. *et al.* Topological photonics. *Rev. Mod. Phys.* **91**, 015006 (2019).
4. Monticone, F. & Alu, A. Metamaterial, plasmonic and nanophotonic devices. *Reports on Prog. Phys.* **80**, 036401 (2017).
5. Kim, M., Jacob, Z. & Rho, J. Recent advances in 2d, 3d and higher-order topological photonics. *Light. Sci. & Appl.* **9**, 1–30 (2020).
6. Yang, Y. *et al.* Terahertz topological photonics for on-chip communication. *Nat. Photonics* **14**, 446–451 (2020).
7. Rider, M. S. *et al.* A perspective on topological nanophotonics: current status and future challenges. *J. Appl. Phys.* **125**, 120901 (2019).
8. Proctor, M., Huidobro, P. A., Maier, S. A., Craster, R. V. & Makwana, M. P. Manipulating topological valley modes in plasmonic metasurfaces. *Nanophotonics* **9**, 657–665 (2020).
9. Yablonovitch, E. Photonic crystals. *J. Mod. Opt.* **41**, 173–194 (1994).
10. Li, C.-A. & Wu, S.-S. Topological states in generalized electric quadrupole insulators. *Phys. Rev. B* **101**, 195309 (2020).
11. Yablonovitch, E. Photonic band-gap structures. *JOSA B* **10**, 283–295 (1993).
12. Haldane, F. D. M. & Raghu, S. Possible realization of directional optical waveguides in photonic crystals with broken time-reversal symmetry. *Phys. Rev. Lett.* **100**, 013904 (2008).
13. Moore, J. E. The birth of topological insulators. *Nature* **464**, 194–198 (2010).
14. Yue, Z., Wang, X. & Gu, M. Topological insulator materials for advanced optoelectronic devices. *Adv. Topol. Insulators* 45–70 (2019).
15. He, Q., Zaquine, I., Roosen, G. & Frey, R. Bragg diffraction in thin 2d refractive index modulated semiconductor samples. *JOSA B* **26**, 390–396 (2009).
16. Ebbesen, T. W., Lezec, H. J., Ghaemi, H., Thio, T. & Wolff, P. A. Extraordinary optical transmission through sub-wavelength hole arrays. *Nature* **391**, 667–669 (1998).
17. Poddubny, A., Miroshnichenko, A., Slobozhanyuk, A. & Kivshar, Y. Topological majorana states in zigzag chains of plasmonic nanoparticles. *ACS Photonics* **1**, 101–105 (2014).

18. Karch, A. Surface plasmons and topological insulators. *Phys. Rev. B* **83**, 245432 (2011).

19. Leykam, D., Bliokh, K. Y. & Nori, F. Edge modes in two-dimensional electromagnetic slab waveguides: Analogs of acoustic plasmons. *Phys. Rev. B* **102**, 045129 (2020).

20. Bliokh, K. Y., Leykam, D., Lein, M. & Nori, F. Topological non-hermitian origin of surface maxwell waves. *Nat. Commun.* **10**, 1–7 (2019).

21. Kim, D. S. *et al.* Microscopic origin of surface-plasmon radiation in plasmonic band-gap nanostructures. *Phys. Rev. Lett.* **91**, 143901 (2003).

22. Kelf, T. A., Sugawara, Y., Baumberg, J. J., Abdelsalam, M. & Bartlett, P. N. Plasmonic band gaps and trapped plasmons on nanostructured metal surfaces. *Phys. Rev. Lett.* **95**, 116802 (2005).

23. Kocabas, A., Ertas, G., Senlik, S. S. & Aydinli, A. Plasmonic band gap structures for surface-enhanced raman scattering. *Opt. Express* **16**, 12469–12477 (2008).

24. Biener, G., Dahan, N., Niv, A., Kleiner, V. & Hasman, E. Highly coherent thermal emission obtained by plasmonic bandgap structures. *Appl. Phys. Lett.* **92**, 081913 (2008).

25. Bozhevolnyi, S. I., Erland, J., Leosson, K., Skovgaard, P. M. W. & Hvam, J. M. Waveguiding in surface plasmon polariton band gap structures. *Phys. Rev. Lett.* **86**, 3008–3011 (2001).

26. Okamoto, T., H'Dhili, F. & Kawata, S. Towards plasmonic band gap laser. *Appl. Phys. Lett.* **85**, 3968–3970 (2004).

27. Grande, M. *et al.* Experimental demonstration of a novel biosensing platform via plasmonic band gap formation in gold nanopatch arrays. *Opt. Express* **19**, 21385–21395 (2011).

28. Shitrit, N., Bretner, I., Gorodetski, Y., Kleiner, V. & Hasman, E. Optical spin hall effects in plasmonic chains. *Nano Lett.* **11**, 2038–2042 (2011).

29. Shitrit, N. *et al.* Spin-optical metamaterial route to spin-controlled photonics. *Science* **340**, 724–726 (2013).

30. Chervy, T. *et al.* Room temperature chiral coupling of valley excitons with spin-momentum locked surface plasmons. *ACS Photonics* **5**, 1281–1287 (2018).

31. Pancharatnam, S. Generalized theory of interference and its applications. In *Proceedings of the Indian Academy of Sciences-Section A*, vol. 44, 398–417 (Springer, 1956).

32. Berry, M. V. Quantal phase factors accompanying adiabatic changes. *Proc. Royal Soc. London. A. Math. Phys. Sci.* **392**, 45–57 (1984).

33. Drezet, A. *et al.* Leakage radiation microscopy of surface plasmon polaritons. *Mater. Sci. Eng. B* **149**, 220–229 (2008).

34. Liu, J.-Q. *et al.* A wide bandgap plasmonic bragg reflector. *Opt. Express* **16**, 4888–4894 (2008).

35. Cohen, E. *et al.* Geometric phase from aharonov–bohm to pancharatnam–berry and beyond. *Nat. Rev. Phys.* **1**, 437–449 (2019).

36. Biener, G., Niv, A., Kleiner, V. & Hasman, E. Formation of helical beams by use of pancharatnam–berry phase optical elements. *Opt. Lett.* **27**, 1875–1877 (2002).

37. Bliokh, K. Y., Gorodetski, Y., Kleiner, V. & Hasman, E. Coriolis effect in optics: unified geometric phase and spin-hall effect. *Phys. Rev. Lett.* **101**, 030404 (2008).

38. Bliokh, K. Y. Geometrical optics of beams with vortices: Berry phase and orbital angular momentum hall effect. *Phys. Rev. Lett.* **97**, 043901 (2006).

39. Bomzon, Z., Biener, G., Kleiner, V. & Hasman, E. Space-variant pancharatnam–berry phase optical elements with computer-generated subwavelength gratings. *Opt. Lett.* **27**, 1141–1143 (2002).

40. Kang, M., Feng, T., Wang, H.-T. & Li, J. Wave front engineering from an array of thin aperture antennas. *Opt. Express* **20**, 15882–15890 (2012).

41. Katardjiev, I., Carter, G. & Nobes, M. The application of the huygens principle to surface evolution in inhomogeneous, anisotropic and time-dependent systems. *J. Phys. D: Appl. Phys.* **22**, 1813 (1989).

42. Niv, A., Biener, G., Kleiner, V. & Hasman, E. Manipulation of the pancharatnam phase in vectorial vortices. *Opt. Express* **14**, 4208–4220 (2006).

Acknowledgements

We acknowledge the Israeli Ministry of Science Technology and Space for a financial support.

Author contributions statement

E.D.E., L.S. and M. F. have conducted the experiments, analyzed the results and contributed to the writing. M.F. performed the numerical simulations. All authors reviewed the manuscript.

Additional information

Competing interests (The authors declare no competing interests).

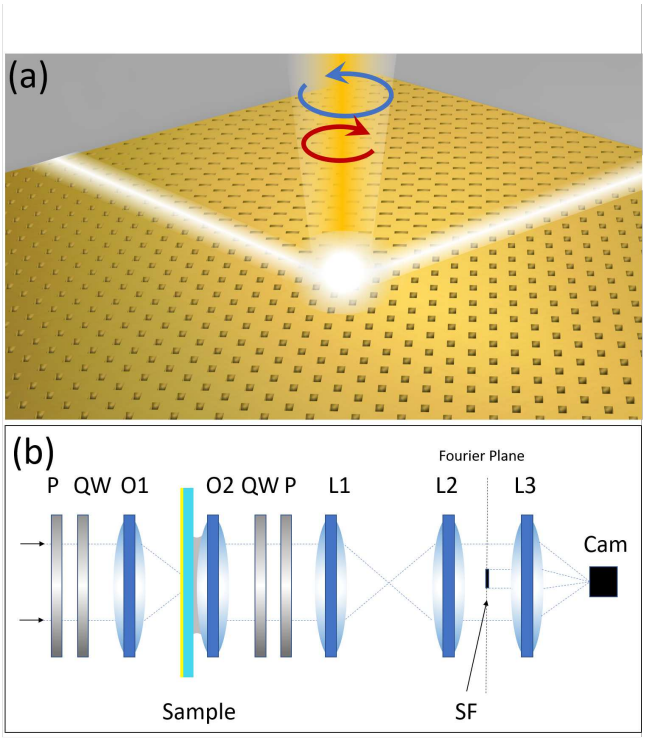

Figure 1. Schematic of optical interaction with metasurface and experimental setup. (a) Right and left polarized light incident on plasmonic grating. (b) The 780nm laser beam is polarized using a polarizer (P) and a quarter-wave plate (QW), and then focused by a 20X objective (O1) with NA = 0.25. The leakage radiation is collected by the second objective (O2, NA = 1.25, 100X) and imaged through the lenses (L1-3) at the camera (Cam). A spatial filter (SF) is used in the secondary Fourier plane to filter out the direct transmission.

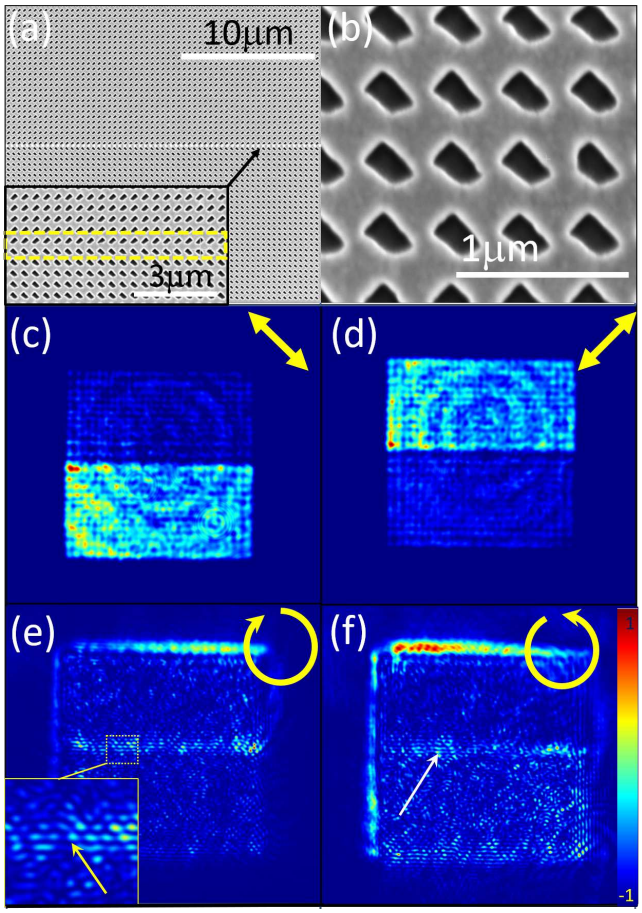

Figure 2. Experimental manifestation of the topological SP mode. (a, b) SEM images of the PlC lattice. Inset in (a) shows the boundary between $+45^\circ$ and -45° domains. (c, d) The transmitted intensity distribution of the sample when illuminated with linear polarization at $\pm 45^\circ$. (e, f) The measured distributions for the incident right and left CP illumination.

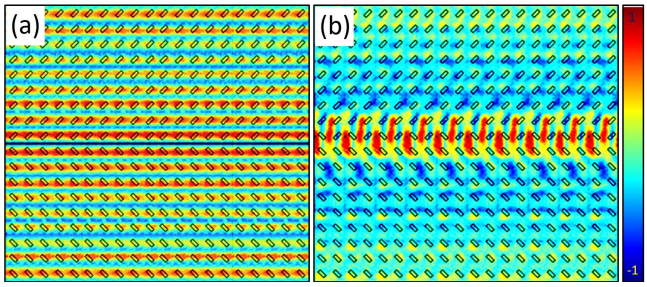

Figure 3. Plasmonic edge modes simulated by the Comsol Multiphysics software. The colormap represents the field amplitude in the 200 nm vicinity of the sample surface. (a) The sample comprises of two $\pm 45^\circ$ domains with a simple boundary and (b) the domains are separated by a zig-zag boundary.

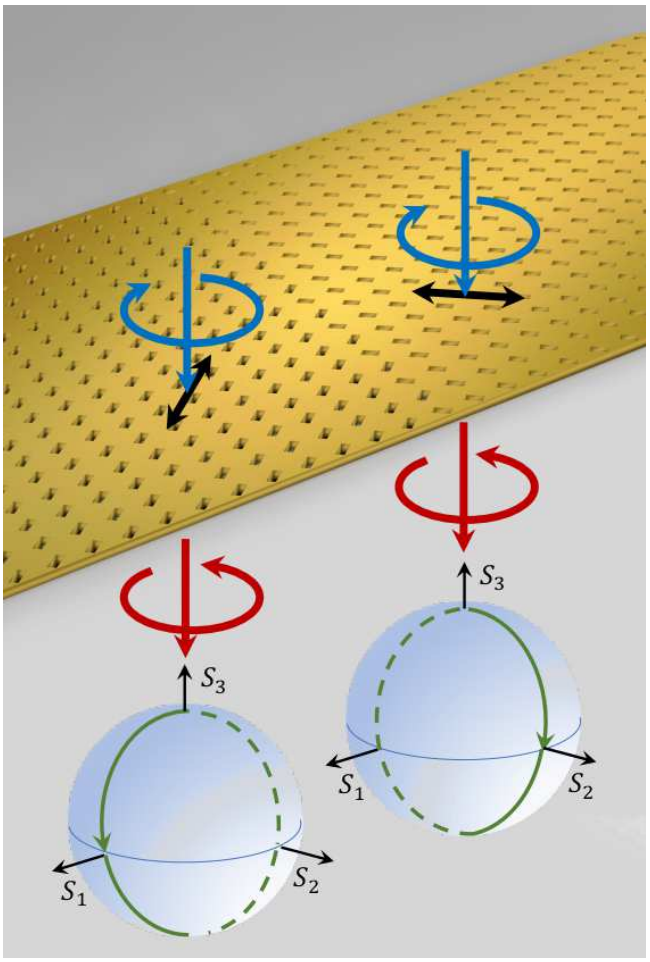

Figure 4. Artistic rendition of the topological Berry phase. The illumination of the Bragg lattice with an anisotropic aperture leads to the serial polarization state manipulation that is depicted as a path on the surface of the Poincaré sphere. The abrupt change in the aperture orientation results in the topological (Berry) phase jump equal to the area enclosed by the two paths.

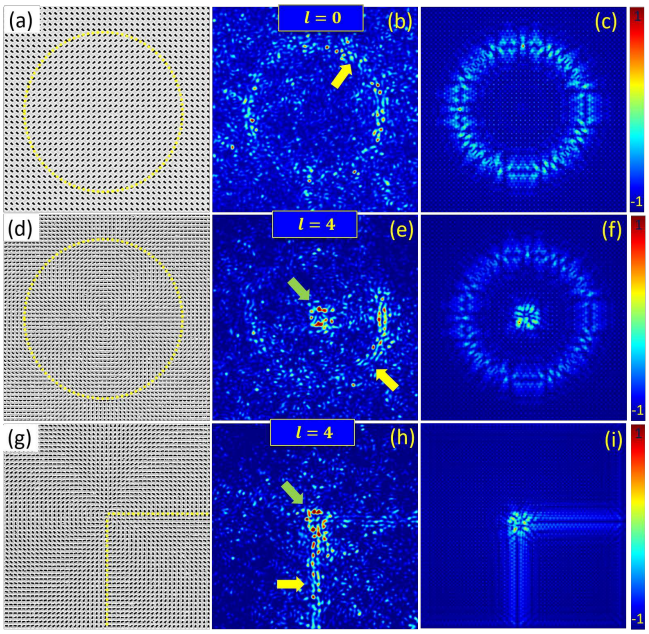

Figure 5. Experimental and calculated SP edge state along the zig-zag boundaries. (a, d) SEM images of the PlC lattice (the domain boundary is marked with the dashed frame). (b,e) The measured transmitted intensity distribution on the sample surface in comparison with (c, f) the distributions calculated using our Matlab solver. Yellow arrows indicate the guided plasmonic mode.

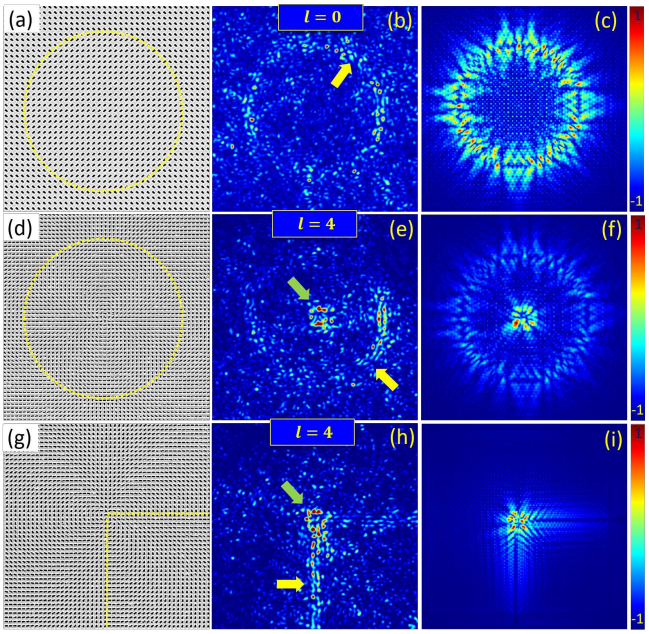

Figure 6. Study of plasmonic metasurfaces with non-trivial topology. The SEM images of the structures are given in (a, d, g) and the measured intensity distribution achieved in our LR system is presented in (b, e, h). The structure in (a) is comprised of two trivial topological phases defined by $\theta = \pm 45^{\circ}$ separated by a circular boundary of the radius $\rho = 10\mu m$. The structure in (e) consists of apertures whose local orientation rotates with topological order $m = 2$ (see details in the text) but having a $\pi/2$ jump along the same circular boundary. The structure in (h) is similar to the one in (e) but the topology change occurs at the lower right corner. (c, f, i) Field amplitude distributions simulated by the Matlab solver.

Figures

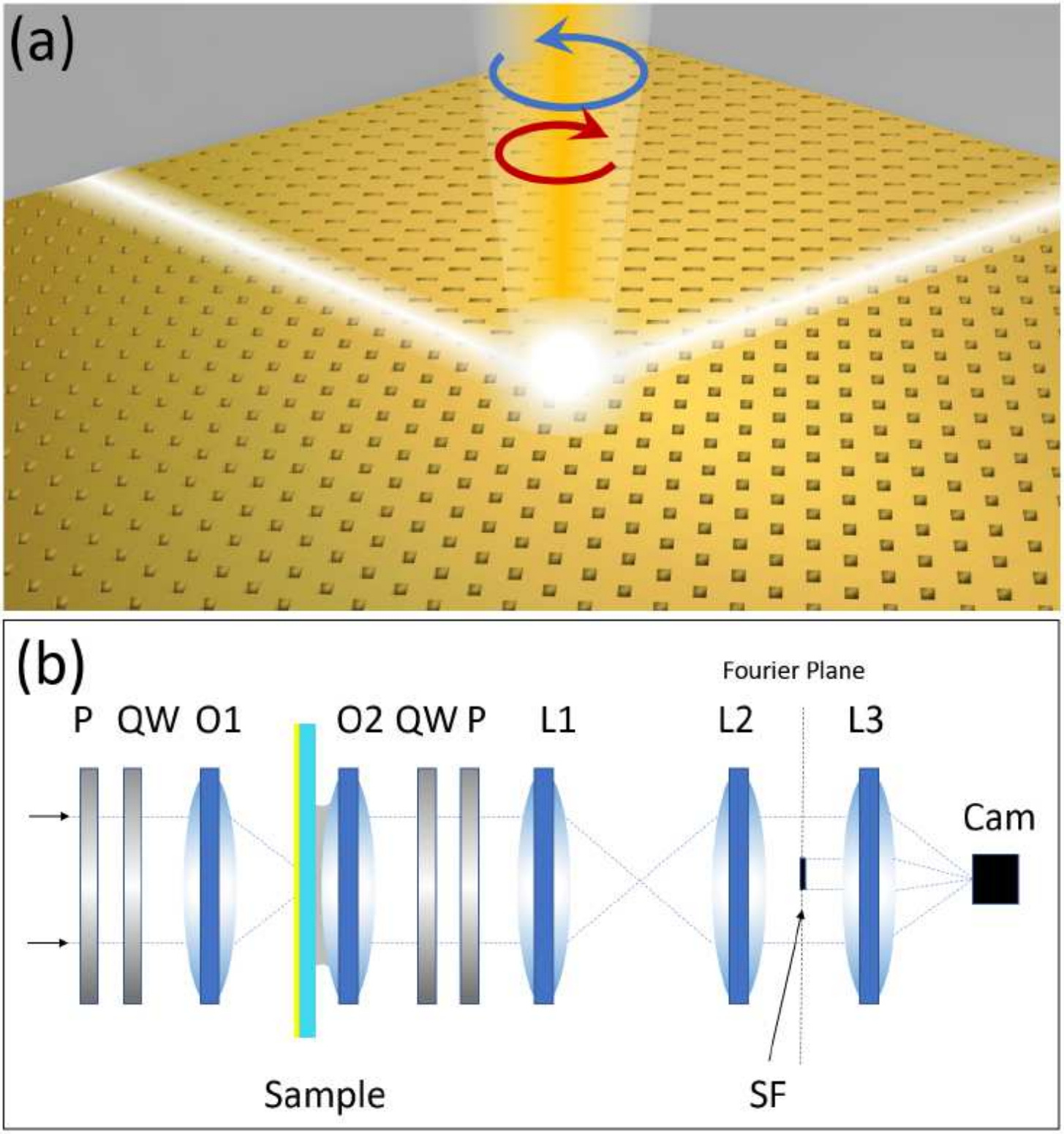

Figure 1

Schematic of optical interaction with metasurface and experimental setup. (a) Right and left polarized light incident on plasmonic grating. (b) The 780nm laser beam is polarized using a polarizer (P) and a quarter-wave plate (QW), and then focused by a 20X objective (O1) with NA = 0.25. The leakage radiation

is collected by the second objective (O2, NA = 1.25, 100X) and imaged through the lenses (L1-3) at the camera (Cam). A spatial filter (SF) is used in the secondary Fourier plane to filter out the direct transmission.

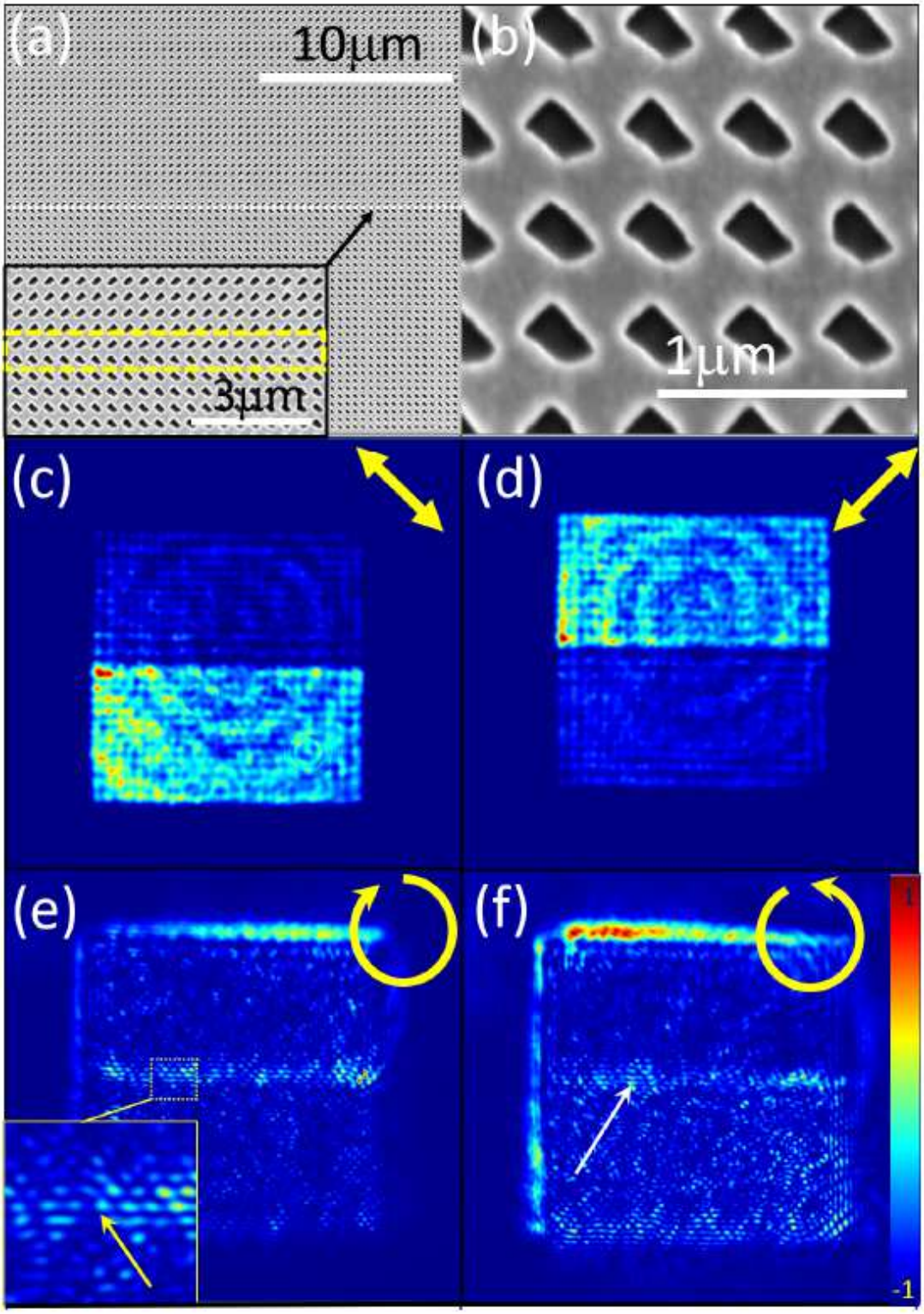

Figure 2

Experimental manifestation of the topological SP mode. (a, b) SEM images of the PIC lattice. Inset in (a) shows the boundary between +45° and −45° domains. (c, d) The transmitted intensity distribution of the

sample when illuminated with linear polarization at ±45°. (e, f) The measured distributions for the incident right and left CP illumination.

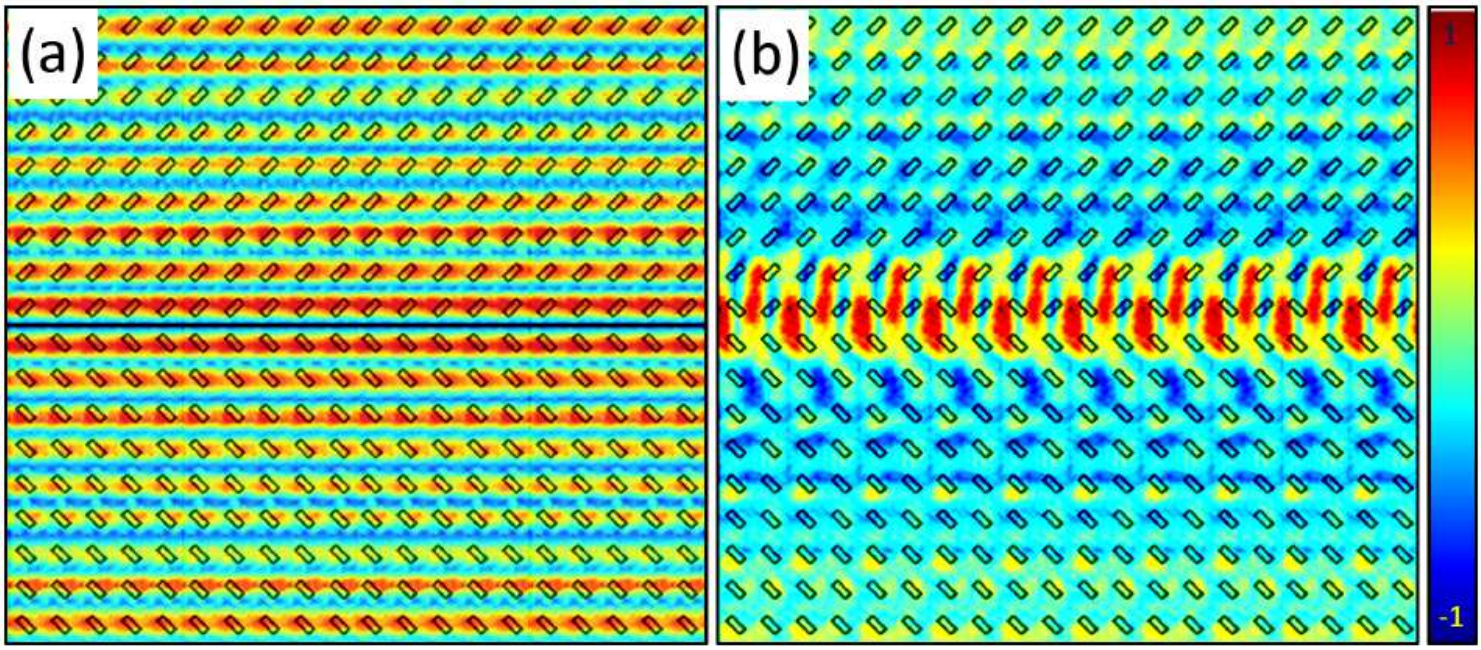

Figure 3

Plasmonic edge modes simulated by the Comsol Multiphysics software. The colormap represents the field amplitude in the 200 nm vicinity of the sample surface. (a) The sample comprises of two ±45° domains with a simple boundary and (b) the domains are separated by a zig-zag boundary.

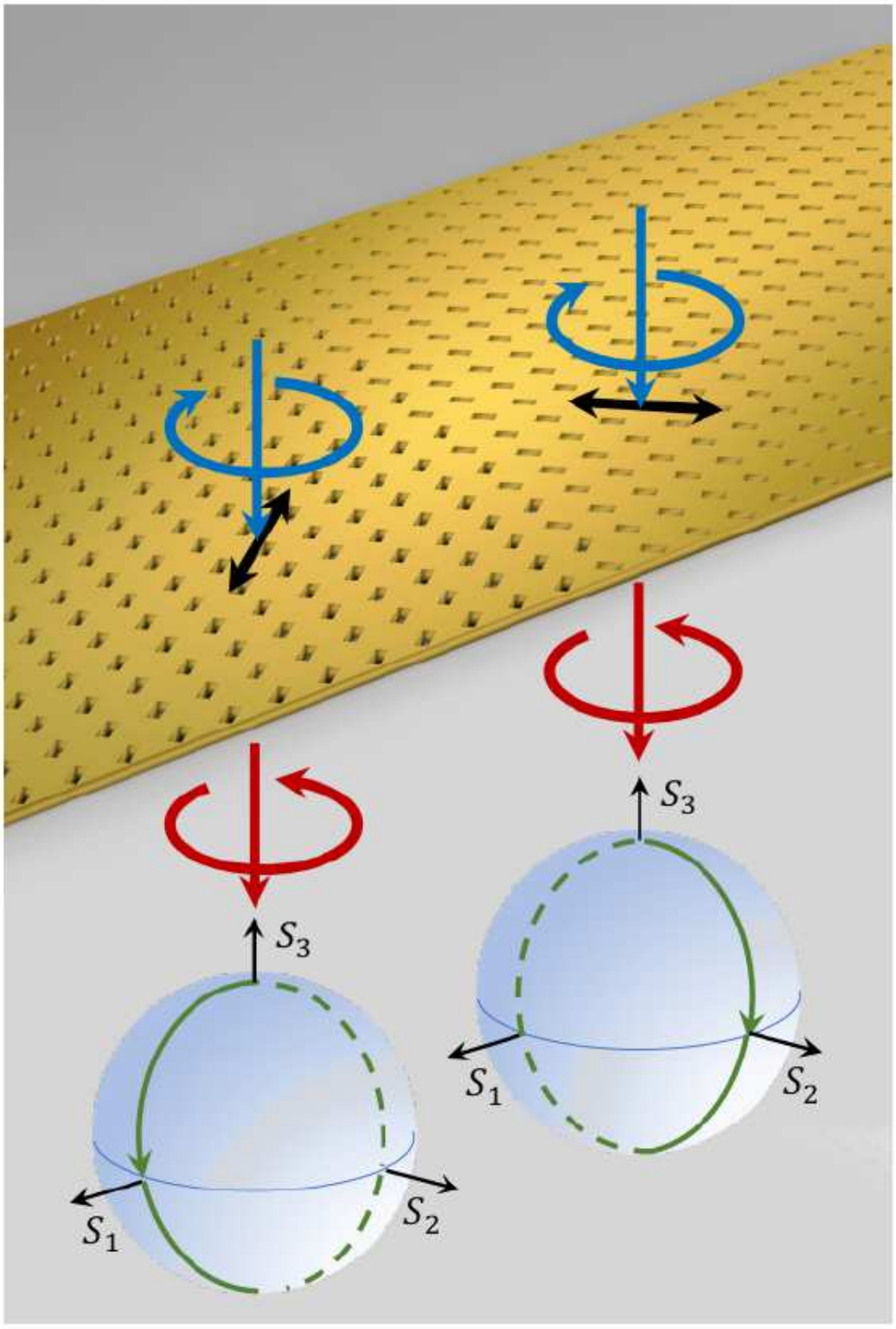

Figure 4

Artistic rendition of the topological Berry phase. The illumination of the Bragg lattice with an anisotropic aperture leads to the serial polarization state manipulation that is depicted as a path on the surface of the Poincaré sphere. The abrupt change in the aperture orientation results in the topological (Berry) phase jump equal to the area enclosed by the two paths.

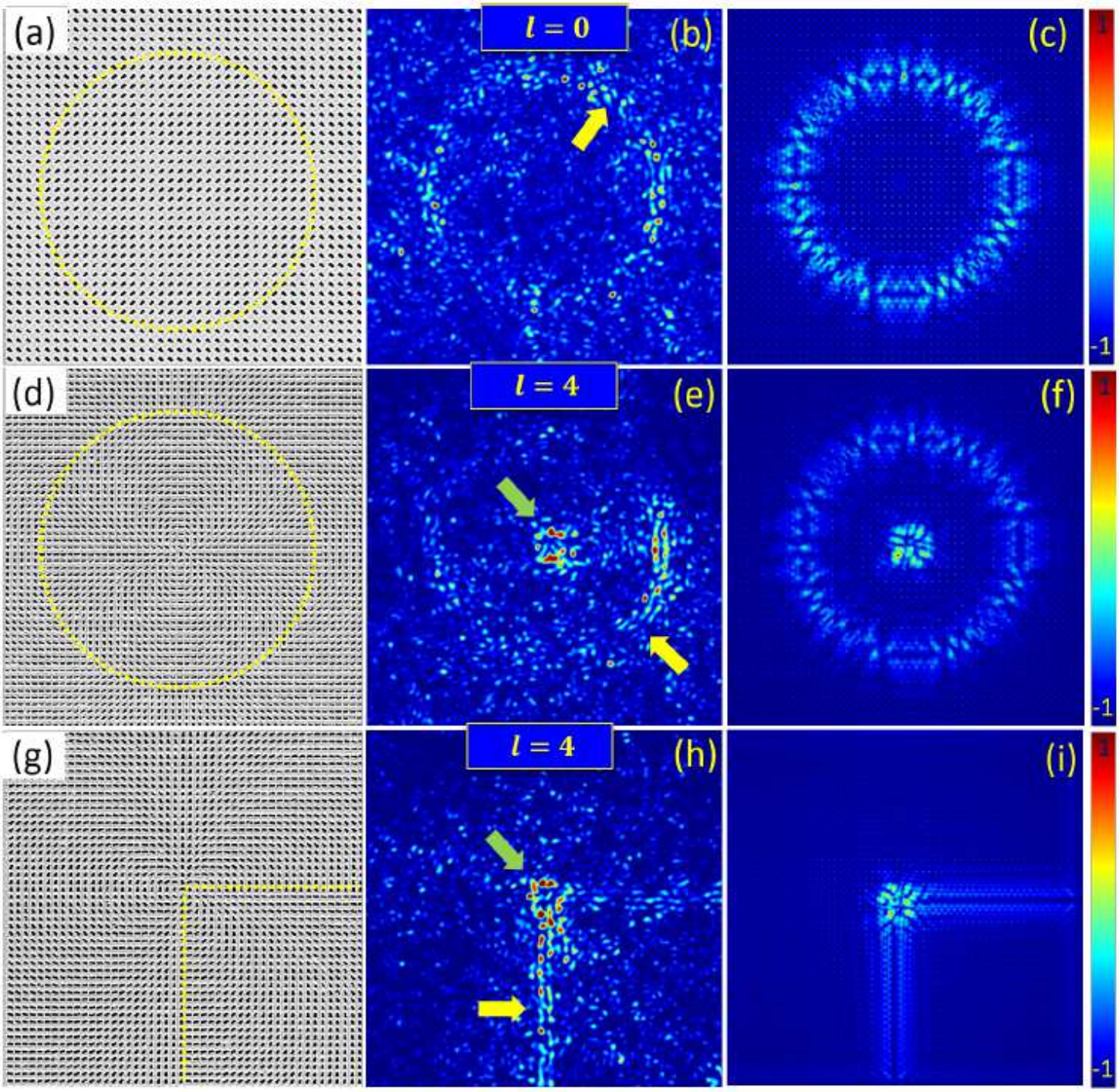

Figure 5

Experimental and calculated SP edge state along the zig-zag boundaries. (a, d) SEM images of the PIC lattice (the domain boundary is marked with the dashed frame). (b,e) The measured transmitted intensity distribution on the sample surface in comparison with (c, f) the distributions calculated using our Matlab solver. Yellow arrows indicate the guided plasmonic mode.

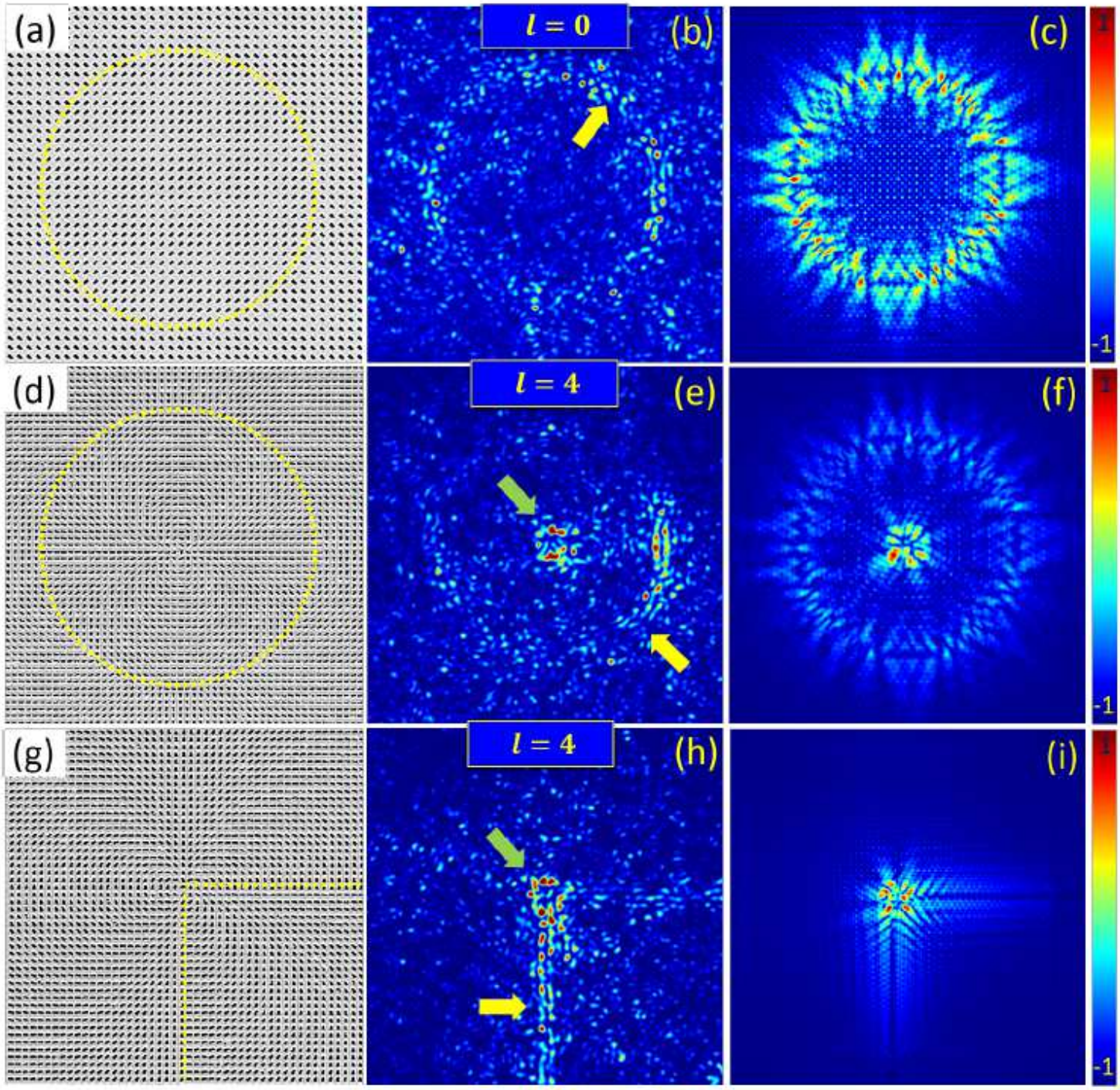

Figure 6

Study of plasmonic metasurfaces with non-trivial topology. The SEM images of the structures are given in (a, d, g) and the measured intensity distribution achieved in our LR system is presented in (b, e, h). The structure in (a) is comprised of two trivial topological phases defined by θ = ±45 separated by a circular boundary of the radius ρ = 10μm. The structure in (e) consists of apertures whose local orientation rotates with topological order m = 2 (see details in the text) but having a π/2 jump along the same circular boundary. The structure in (h) is similar to the one in (e) but the topology change occurs at the lower right corner. (c, f, i) Field amplitude distributions simulated by the Matlab solver.